THE AMERICAN SOCIETY OF MECHANICAL ENGINEERS
345 E. 47th St., New York, N.Y. 10017

97-GT-25

THE INFLUENCE OF COOLANT SUPPLY GEOMETRY ON FILM COOLANT EXIT FLOW AND SURFACE ADIABATIC EFFECTIVENESS

Steven W. Burd and Terrence W. Simon

Heat Transfer Laboratory
University of Minnesota
Minneapolis, MN 55455, U.S.A.

ABSTRACT

Experimental hot-wire anemometry and thermocouple measurements are taken to document the sensitivity which film cooling performance has to the hole length and the geometry of the plenum which supplies cooling flow to the holes. This sensitivity is described in terms of the effects these geometric features have on hole-exit velocity and turbulence intensity distributions and on adiabatic effectiveness values on the surface downstream. These measurements were taken under high freestream turbulence intensity (12%) conditions, representative of operating gas turbine engines. Coolant is supplied to the film cooling holes by means of (1) an unrestricted plenum, (2) a plenum which restricts the flow approaching the holes, forcing it to flow co-current with the freestream, and (3) a plenum which forces the flow to approach the holes counter-current with the freestream. Short-hole (L/D=2.3) and long-hole (L/D=7.0) comparisons are made. The geometry has a single row of film cooling holes with 35°-inclined streamwise injection. The film cooling flow is supplied at the same temperature as that of the freestream for hole-exit measurements and 10°C above the freestream temperature for adiabatic effectiveness measurements, yielding density ratios in the range 0.96-1.0. Two coolant-to-freestream velocity ratios, 0.5 and 1.0, are investigated. The results document the effects of (1) supply plenum geometry, (2) velocity ratio, and (3) hole L/D.

NOMENCLATURE

D	diameter of the film cooling holes
DR	density ratio (ρ_j/ρ_∞)
FSTI	freestream turbulence intensity (u_{rms}/U_o)
h	height of the film cooling delivery channel
I	momentum flux ratio (DR·VR^2)
k	thermal conductivity
L	length of the film cooling delivery tube
M	blowing mass flux ratio (DR·VR)
Re_D	Reynolds number based on U_{hole} and D
Re_θ	Reynolds number based on U_o and θ
T_∞	freestream temperature
T_j	bulk mean temperature of the coolant
T_{aw}	adiabatic wall temperature of the film-cooled surface
TI	local effective turbulence intensity (u_{rms}/U_{eff})
U_{eff}	mean effective velocity as seen by a hot-wire parallel to the film-cooled surface and normal to the freestream
U_{hole}	bulk mean velocity of the coolant flow within hole
U_o	time-averaged freestream velocity
u'	instantaneous effective velocity fluctuation
u_{rms}	rms fluctuation of the effective velocity ($\sqrt{\overline{u'^2}}$)
VR	ratio of coolant bulk mean velocity to freestream velocity (U_{hole}/U_o)
x	streamwise distance from the center of the hole
y	distance normal to the test wall
z	lateral distance from the center of the middle hole

Greek:

θ	momentum thickness
δ	hydrodynamic boundary layer thickness (99%)
δ_T	thermal boundary layer thickness
δ^*	displacement thickness
η	adiabatic film cooling effectiveness
η_{av}	laterally-averaged adiabatic film cooling effectiveness
ρ_j	film coolant density
ρ_∞	freestream air density

Superscripts:

$\overline{\ }$	time-averaged

Presented at the International Gas Turbine & Aeroengine Congress & Exhibition
Orlando, Florida — June 2–June 5, 1997

INTRODUCTION

Film cooling is commonly used to prevent distress and failure of turbine blades in gas turbine engines which would result from excessive operating temperatures. With film cooling, cool air is bled from the compressor, ducted to the internal chambers of the turbine blades, and discharged through small holes in the blade walls. This air provides a thin, cool, insulating blanket along the external surface of the turbine blade. The cooling effectiveness is dependent upon the approach flow turbulence; the film cooling flow temperature, velocity distribution, and turbulence; and the blade and film cooling hole geometries.

Film cooling literature is extensive. It concentrates primarily on surface and flowfield measurements. Surface measurements include film cooling effectiveness values and heat transfer coefficients whereas flowfield measurements include velocity and turbulence intensity distributions and turbulent shear stresses. Such measurements directly support cooling design parameter choices and the development of design models.

There are three important aspects to the present study - high freestream turbulence, short film cooling holes, and hole supply plenum variations. Some previous studies which have addressed these aspects will now be discussed.

High Freestream Turbulence

Since measurements of combustor exit flows by Goebel et al. (1993) indicate turbulence levels of 8-12%, elevated turbulence is considered to be an important factor. A majority of film cooling studies in the literature have been conducted with FSTI<1%. Launder and York (1974) found no influence of 4% FSTI. Brown and Saluja (1979) and Brown and Minty (1975) found losses in cooling effectiveness for FSTI ranging from 2 to 8%. Mehendale and Han (1990) studied the effect of mainstream turbulence (FSTI=0.75% to 12.9%) on leading edge film cooling and noted effectiveness losses at low blowing rates with elevated FSTI. Jumper et al. (1991), investigating the influence of high (14-17% vs. 0.5%) freestream turbulence on film cooling effectiveness, found a faster streamwise decay in film cooling effectiveness with elevated FSTI than with low FSTI. Bons et al. (1994) documented film cooling effectiveness with FSTI=0.9%, 6.5%, 12%, and 17.5%, several velocity ratios, and L/D=3.5. High FSTI enhanced mixing, reduced film cooling effectiveness (by up to 70%) in the region directly downstream of the injection hole, and increased film cooling effectiveness 50-100% in the near-hole regions between holes. Schmidt and Bogard (1996) found changes in effectiveness to depend on the coolant-to-freestream momentum flux ratio when FSTI is increased. Elevated FSTI reduced effectiveness downstream of the hole for film cooling with low momentum flux ratios but increased values when momentum flux ratios were large. Flowfield measurements were presented by MacMullin et al. (1989) for FSTI in the range of 7 to 18%. Gogineni et al. (1996) used two-color particle image velocimetry to investigate velocity and vorticity fields with 35°-inclined, single-row injection and FSTI values of 1 to 17%. Wang et al. (1996) used three-wire anemometry to document the flowfield just downstream of injection for FSTI=0.5% and 12%. Computed from the data were the eddy viscosity in the lateral and wall-normal directions, and the ratio of the two, the anisotropy of turbulent transport. Burd et al. (1996) detailed some of the fundamental differences that exist between film cooling flows under high (12%) and low (0.5%) FSTI. They documented the enhanced mixing with elevated FSTI.

Short Delivery Length

Historically, film cooling studies have incorporated long-hole delivery. In recent years, researchers have elected to use shorter length-to-diameter ratios which are more representative of turbines. With a very short L/D of 1.75, Sinha et al. (1991) studied film cooling effectiveness downstream of holes with variable DR, 35°-streamwise injection and low FSTI. Schmidt et al. (1994) investigated film cooling performance with L/D=4.0 to note the differences in adiabatic effectiveness that exist between round streamwise injection and compound-angle injection with round and shaped holes. Their studies were performed at DR=1.6 and M=0.5-2.5. Kohli and Bogard (1995) expanded L/D to 2.8 and 3.5 to investigate 35°- and 55°- streamwise injection with DR=1.6. Similarly, L/D=3.5 was used by Bons et al. (1994) and Pietrzyk et al. (1989, 1990) for studies of 35°-streamwise injection.

Differences between short- and long-hole injection have been numerically investigated as well. Leylek and Zerkle (1994) performed three-dimensional, Navier-Stokes computation and compared their results to the experiments of Pietrzyk et al. (1989, 1990) and Sinha et al. (1991). They found that film cooling exit flow contains counter-rotating vortices and displays local jetting effects. They suggested that film cooling experiments with long L/D may be misleading for engine applications. Studies at the University of Minnesota have also investigated the role of L/D in film cooling. Burd et al. (1996) conducted experimental studies with short (L/D=2.3) and long (L/D=7.0) hole delivery lengths showing that L/D significantly influences the hole-exit velocity profiles and the manner by which the coolant and freestream flows interact. In a numerical study, Berhe and Patankar (1996) computed the influence of hole L/D and reported similar findings.

Hole Supply Plenum Variations

Recent studies have been with film cooling delivery flow geometries that are representative of those in actual airfoil designs. Byerley et al. (1988, 1992) and Gillespie et al. (1994) measured heat transfer from the supply plenum wall near the entrance to film cooling holes. These studies incorporated different angles of inclination of the holes with the flow directed to the holes through a two-dimensional channel of height-to-diameter ratio, h/D=2.27. They found significant heat transfer enhancement due to the discrete film cooling holes. Thole et al. (1996b) and Wittig et al. (1996) also used a channeled-flow delivery to study the effects of hole shapes, including those with expanded exits, on flowfield and surface heat transfer. Using the same facility, Thole et al. (1996a) investigated the influence of the coolant supply channel velocity on the flowfield at the jet exit and in the freestream. This investigation revealed significant influences of the channel velocity on the hole-exit and downstream flowfield velocities. In these studies, the flow was supplied to the holes parallel to and in the same direction as the freestream. The supply channel had

h/D=2.0. Berhe and Patankar (1996) computed the role of supply plenum height and flow direction on film cooling performance. They found that the plenum flow direction has an effect on film cooling performance when h/D≤2.0.

The Present Study

Over the years, researchers have restricted their test cases to a limited number of film cooling parameters. Although each has contributed to general understanding, differences in test and flow configurations make comparing results of one with another difficult. Specifically, few direct comparisons of the roles of L/D and coolant supply configuration can be clearly made for they were often conducted in separate facilities and under different conditions. In a recent paper by Burd et al. (1996), the results of an experimental study of the effects of both the film cooling hole length-to-diameter ratio and FSTI on the downstream flowfield were presented, all from a common facility. These cases were with cooling supply to the holes from a large, unrestricted plenum. Two L/D values and two FSTI levels, with VR=1.0, were presented. The focus of that paper was on differences between long and short L/D delivery and between low and high FSTI. In the present paper, further differences between the two L/D cases at high FSTI are discussed. In addition, when holes are short, concern arises about the effect of the geometry of the plenum which supplies the film coolant to these holes. In the present paper, the effect of plenum geometry is discussed.

Mean velocity, turbulence intensity, and surface adiabatic effectiveness distributions are documented for four different film cooling injection configurations under high freestream turbulence conditions. The configurations are (1) a large, unrestricted delivery plenum and a hole length-to-diameter ratio of 2.3, (2) the same plenum and a hole length-to-diameter ratio of 7.0, (3) a restricted plenum which forces the flow to be co-current with the freestream flow and L/D=2.3, and (4) a restricted plenum with flow counter-current to the freestream flow and L/D=2.3. The velocity and turbulence data are gathered at the exit plane of the film cooling holes. Surface effectiveness data are presented for the downstream film-cooled surface over $1.25 \le x/D \le 10.0$ and $-1.5 \le z/D \le 1.5$.

Of the many parameters which affect film cooling performance, three important effects are not studied in the present paper - (1) surface curvature, (2) density differences between coolant and freestream flows, and (3) variations in the holes' geometries due to manufacturing limitations. These are reserved for later separate effects studies. Regarding the density ratio, it has been shown that data from cases of various density ratio collapse somewhat when the momentum flux ratios, I, match. Cases discussed in this paper show this momentum flux ratio effect.

EXPERIMENTAL TEST FACILITY AND PROCEDURE

Wind Tunnel

The freestream flow is supplied by a high-turbulence facility; a small, blown-type wind tunnel which simulates the flow of a gas turbine combustor (Fig. 1). The facility is described by Wang et al. (1996). The measured freestream turbulence at the 68.6 cm x 12.7 cm nozzle exit is nearly isotropic with intensity, FSTI, and decay rate, d(FSTI)/d(x/D), of approximately 12.3% and 0.12%, respectively. The FSTI level is characteristic of flow exiting the combustor stage in actual gas turbine engines (Goebel et al. 1993). The exit-plane turbulence intensity and mean velocity are uniform to within 2% of their mean values and the integral length scale calculated from a u' power spectrum is 3.3 cm.

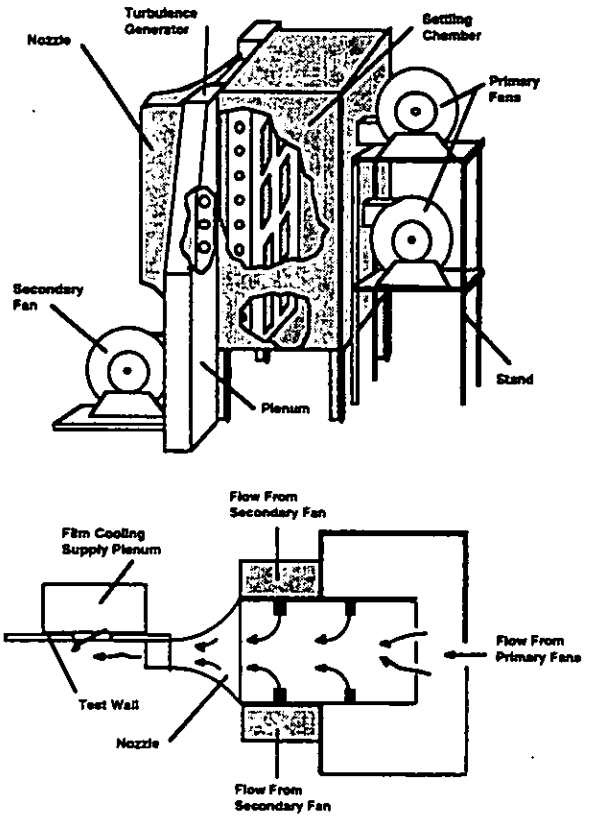

Figure 1: Test Facility

Test Section

The test section (Fig. 1) consists of an upstream plate (25.4 cm x 68.6 cm), the test plate (15.2 cm x 68.6 cm), a downstream plate (91 cm x 68.6 cm), and the film coolant supply system. The upstream plate is fabricated of 9.53 mm-thick cast acrylic. The test plate, x/D=-3.5 to x/D=4.7, is fabricated of 2.54 cm-thick silicon phenolic laminate plate. Silicon phenolic is of low thermal conductivity (k=0.25W/m·K). There is a single column of eleven film cooling holes distributed uniformly across the test plate. Film cooling flow is injected at an angle of 35° with respect to the plate surface in the streamwise direction. The film cooling holes are 1.9 cm in diameter and three diameters apart, center-to-center. The film cooling delivery tubes have a length-to-diameter ratio of either 2.3 or 7.0. The larger allows fully-developed flow within the delivery tubes. The smaller represents film cooling designs in modern airfoils. The downstream plate is fabricated of 9.53 mm-thick acrylic sheet. Polystyrene insulation is placed on the back side of the downstream plate to reduce conduction through the plate.

25

A square-edged, rectangular polycarbonate strip (1.6 mm thick x 13 mm wide x 68.6 cm long) is attached to the upstream plate as a boundary layer trip. Its upstream edge is 21.1 cm upstream of the hole centers. In all experiments, the freestream flow is maintained at a nominal velocity of 11.0 m/s, while the bulk coolant velocity is varied to achieve VR=0.5 (Re_D~6,500) and 1.0 (Re_D~13,000). The approach flow conditions of the freestream at x/D=-4.0 are δ/D=1.10, δ^*/D=0.094, θ/D=0.073, Re_θ=960, and FSTI=12%. Details are given by Burd et al. (1996). Film cooling flow is supplied by a fan through a metering section with two laminar flow meters and a large, unrestricted supply plenum. For measurements of adiabatic effectiveness, the coolant supply flow is heated by a coil resistance heater to 10°C above the freestream temperature with hole-to-hole temperature variations of less than 0.2°C.

Instrumentation

A single-sensor (TSI model 1218-T1.5) hot-wire probe and TSI IFA 100 bridge are used to obtain the velocity and turbulence data. A total of 4096 data points was recorded for each measurement location over a sampling time of 40 seconds.

Thermocouples were used to measure the freestream and coolant bulk temperatures. A traversing thermocouple probe, constructed by You (1986), following the design of Blackwell and Moffat (1975), was used to take temperature profiles in the freestream-coolant interaction region downstream of the holes. Two prongs support a thermocouple wire which is butt-welded at its mid-span and is slightly bowed, allowing very near-wall measurements. All thermocouple wires are 76μm diameter, type E (chromel-constantan). The small diameter was chosen to minimize conduction through the thermocouple leads. All thermocouples were referenced to the same isothermal box which was referenced to an ice bath.

A Hewlett Packard Model 3412A Data Acquisition Unit was used to acquire thermocouple voltages. A total of 100 readings of each thermocouple voltage was taken over a period of 50 seconds for the measurements of the adiabatic wall temperature, freestream temperature, and coolant jet temperature. Only mean temperatures are discussed. Other thermocouples, whose signals were more steady, were sampled less frequently.

An automated, two-dimensional traversing system allowed high-spatial-resolution (0.025 mm capability) measurements in the wall-normal and spanwise directions. Movement in the streamwise direction was manual.

Experimental Procedure

Hot-Wire Measurements. Measurements about the hole-exit plane (Fig. 2) were taken using single-wire, hot-wire anemometry by traversing the sensor parallel to the film-cooled surface and normal to the freestream flow over the exit of the film cooling hole. The mean velocity and velocity fluctuations are effective quantities as seen by the hot-wire and are not resolved into their wall-normal and streamwise components.

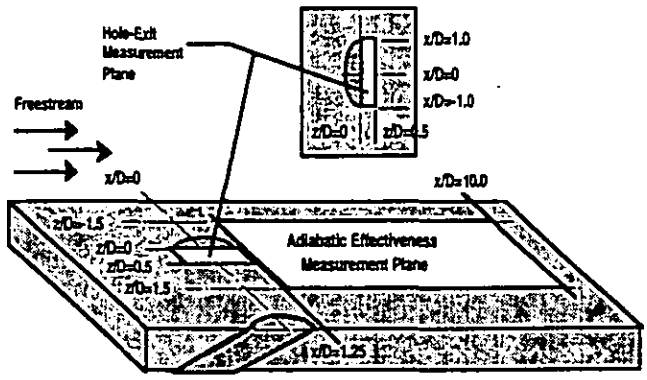

Figure 2: Experimental Measurement Planes for Hole-exit and Adiabatic Effectiveness Measurements

Temperatures and Adiabatic Effectiveness. The performance of the film cooling scheme is given in terms of adiabatic effectiveness, η, defined as:

$$\eta = (T_{aw}-T_\infty)/(T_j-T_\infty)$$

To measure η, the wall temperature of an adiabatic surface under the film cooling flow must be measured as well as the bulk mean film cooling jet temperature and the freestream temperature. In the present study, the coolant supply and freestream temperatures are measured using thermocouples immersed in the respective flows. The local adiabatic wall temperature is measured with the traversing thermocouple by extrapolation of the near-wall fluid temperature profile to the wall. Laterally-averaged effectiveness values, η_{av}, are calculated by trapezoidal integration of the laterally-distributed η values at a fixed streamwise position. Local surface adiabatic effectiveness values are measured at six different streamwise positions (x/D=1.25, 2.5, 3.75, 5.0, 7.5, and 10.0) and at 23 laterally-distributed locations ($-1.5 \le z/D \le 1.5$) about a single hole (Fig. 2). The freestream velocity is measured with a single, hot-wire at x/D=-4.0. The coolant hole bulk mean velocity is determined via the use of two laminar flow meters. Prior to taking measurements, the facility was permitted to reach steady state. Generally, this "pre-test" time was 4-5 hours. At steady state, the coolant jet was maintained 10°C above the freestream temperature.

Experimental Uncertainty

Hot-wire uncertainties result from changes in fluid properties between calibration and measurement, near-wall effects, and sensor drift. A standard propagation of uncertainty (Kline and McClintock, 1953) yields 7% at 3 m/s to 5% at 10 m/s. Due to the large sample sizes and long sampling times, stochastic errors fall well below deterministic errors and are negligible in comparison. The rms velocity fluctuation and the mean velocity have nearly the same uncertainties.

Comparisons of mean velocity and turbulence intensity to data by Laufer (1953) in a fully-developed pipe flow are used to corroborate these uncertainty values. Per these data, bias error

contributions on the order of 5% of mean values are reasonable, so long as velocity fluctuation levels remain below 25% of the mean streamwise velocity. Our uncertainties are consistent with previous experience with such measurements and with Yavuzkurt (1984).

Uncertainties in the coolant and freestream temperature are approximately 0.2°C. The measured adiabatic wall temperature is determined by extrapolation of the near-wall fluid temperature profile to the wall. This would normally be trivial since the near-wall flow over the adiabatic wall has a zero gradient and there are several points within this isothermal zone. The measurement is more complex, however, due to a small amount of conduction upstream of the holes that was observed in the temperature profiles. This heated the approach flow in the very near-wall region ($\delta_T/D<0.05$ for $x/D\leq10$) upstream of the holes. Though a small effect throughout the flow, it was observed that this upstream heating influenced the region between the film cooling holes ($z/D<-1.0$ and $z/D>1.0$) where the effectiveness tends to be small. In this region, "false-high" temperature measurements were recorded. As the thermocouple probe was moved further from the wall; an isothermal (variations ≤0.1°C) region was observed. As the probe was moved even further from the wall, mild gradients associated with the coolant-freestream interaction were observed. The effect of this upstream heating was removed from the data by extrapolating the isothermal portion of the temperature profile to the wall, ignoring the very near-wall gradients. With this extrapolation, zero values of η are recorded at locations upstream of the film cooling holes. The magnitude of this compensation varied from a negligible effect on η directly behind the holes to as high as 9% in the region between the holes, where η values are small. Uncertainties in the adiabatic wall temperature are found to be 0.3°C or less. Uncertainties in η, thus, do not exceed 3.2% of the maximum obtainable value of 100%, throughout. Repeatability of η is within 2%. It should be noted that the identification and quantification of the conduction error is a result of measuring the adiabatic wall temperature with a traversing thermocouple probe. It would not have been identified with a thermocouple embedded in the surface. All thermocouples were calibrated using the same methodology and checked regularly against one another to eliminate biases in measured values. All thermocouples were referenced to the same ice bath to minimize uncertainties in temperature differences. Uncertainty in the total coolant mass flow rate is 2.3% and 2.8% for hole-exit and adiabatic effectiveness measurements, respectively. All uncertainties are expressed with 95% confidence.

Table 1: Cases in this Study

CONFIGURATION	VR	L/D
SHORT-HOLE, UNRESTRICTED PLENUM (SHUP)	0.5	2.3
SHORT-HOLE, UNRESTRICTED PLENUM (SHUP)	1.0	2.3
LONG-HOLE, UNRESTRICTED PLENUM (LHUP)	0.5	7.0
LONG-HOLE, UNRESTRICTED PLENUM (LHUP)	1.0	7.0
COUNTER-FLOW DELIVERY	0.5	2.3
COUNTER-FLOW DELIVERY	1.0	2.3
CO-FLOW DELIVERY	0.5	2.3
CO-FLOW DELIVERY	1.0	2.3

Cases Studied

Four different film cooling configurations, listed in Table 1 and shown in Fig. 3, are documented in this study.

The first two configurations are cases with a large, unrestricted plenum such that the coolant is delivered as a "sink" flow to the film cooling holes. The short-hole (Fig. 3a) configuration has L/D=2.3; the long-hole case (Fig. 3b) has L/D=7.0. Data presented herein complement the flowfield data of Burd et al. (1996).

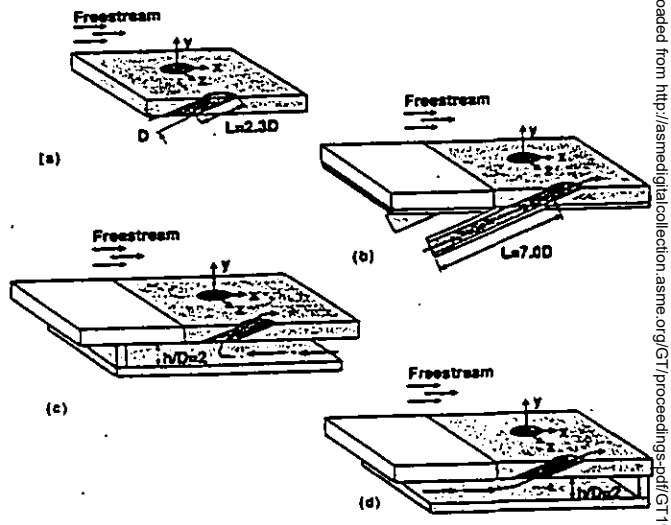

Figure 3: Coolant Delivery Configurations
(a) Short-Hole, Unrestricted Plenum-SHUP,
(b) Long-Hole, Unrestricted Plenum-LHUP,
(c) Counter-Flow Delivery, and (d) Co-Flow Delivery

In actual blades, the coolant is supplied to the cooling holes through channels that are internal to the blade. The geometries of these channels influence this flow. To model the sensitivity of the film cooling flow to the direction of the coolant delivery, two geometries (with L/D=2.3) are investigated. The first geometry (Fig. 3c), "counter-flow," forces the film coolant to approach the film cooling hole counter-current (parallel to but in the opposite direction) with the freestream. The second geometry (Fig. 3d) is "co-flow." These are only two of many delivery possibilities in cooled airfoils. The channel height-to-hole-diameter ratio is 2.0, which is on the short side of the range for current blade designs (1.0 to 10.0). The choice concurs with h/D values used by other researchers (Thole et al., 1996a/1996b; Wittig et al., 1996). The focus herein is to document the differences that may exist with different delivery configurations and to present some of the implications of these differences in terms of adiabatic effectiveness.

EXPERIMENTAL RESULTS

Film cooling results in the literature are excellent for evaluating effectiveness of various schemes. They generally lack auxiliary measurements, such as data to show how the flow emerges

25

from the holes and interacts with the freestream flow, however, to explain their results. This paper presents such data along with film cooling effectiveness data.

The first section of this paper documents the differences that exist between short-hole and long-hole injection while the second highlights differences due to supply plenum geometry. In the latter section, short-hole, unrestricted plenum (SHUP) delivery is the base case to which restricted plenum cases are compared. Both sections present effective velocity and turbulence distributions at the exit plane of the film cooling hole and adiabatic effectiveness values on the downstream surface. They show that the coolant delivery configuration has a significant impact on the hole-exit profiles and, in turn, a substantial effect on adiabatic effectiveness. The main effect is with the delivery hole length, but the plenum geometry effect is not to be ignored.

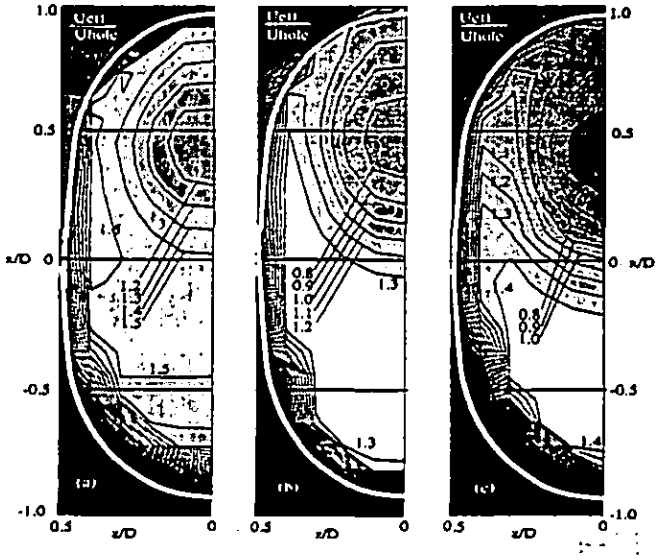

Figure 4: Normalized Mean Effective Velocity Distributions for Short-Hole Injection - (a) VR=0.5, (b) VR=1.0 and (c) U_o=0 m/s and U_{hole} same as (a)
[Approximate outline of hole is indicated by white line].

Hole-Exit Profiles: SHUP Injection

Figure 4 shows contours of mean effective velocities measured at the exit plane of the film cooling hole for short-hole injection. Figure 5 highlights centerline effective velocity and TI distributions for these cases. Profiles with short-hole injection exhibit a prominent "jetting" of the coolant, which is characterized as higher effective velocities in the upstream portion of the hole. In moving toward the downstream side of the hole, the effective velocity decreases rapidly, forming a depression, and then increases steeply near the downstream edge.

Integration of the normalized effective velocities over the entire exit plane yields a value greater than unity. This indicates that the freestream significantly induces the coolant flow. To demonstrate the influence of the freestream on the exit profile versus that attributable to the hole geometry, a hole-exit profile for short hole injection at the same blowing velocity as Fig. 4a but with no freestream flow was taken (Fig. 4c). Integration of this flow over the exit plane yields unity. Comparing Fig. 4a to 4c leads to the conclusion that jetting behavior is inherent to the short-hole geometry and mostly separate from the freestream effect, but that the freestream has an influence in the downstream portion of the flow.

Hole-Exit Profiles: LHUP Injection

With a large, unrestricted delivery plenum and a long hole (L/D=7.0), centerline hole exit profiles, given in Fig. 5, show less jetting than with short holes. At VR=0.5, a near-parabolic profile is observed and the freestream skews the profile towards the downstream edge of the hole. At VR=1.0 (Fig. 5b), the exit profile is less skewed. TI levels in the short-L/D cases are significantly higher than with long-hole injection (Figs. 5a and 5b). In addition, long-hole injection produces a more uniform TI distribution over the film cooling hole. In both cases, the highest TI levels are reported in regions of low velocity. Levels for long-hole injection are more characteristic of those in fully-developed turbulent flows in tubes (Laufer, 1953).

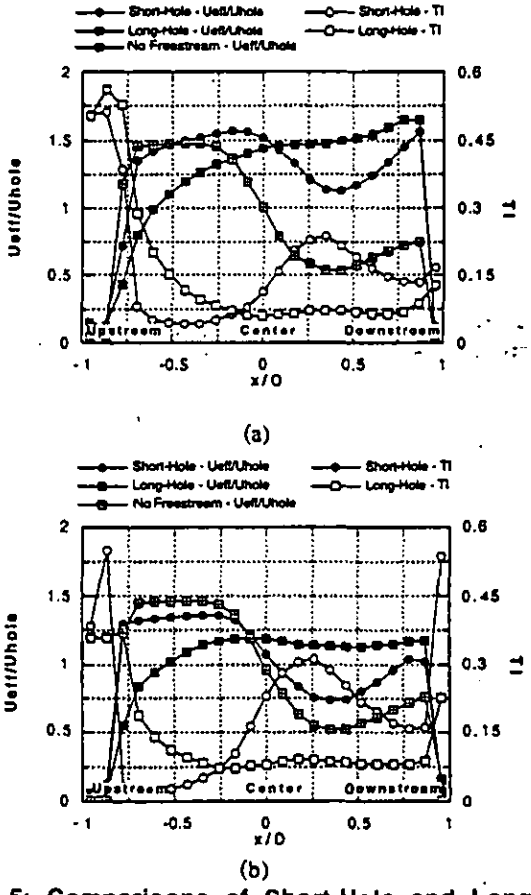

Figure 5: Comparisons of Short-Hole and Long-Hole Normalized Centerline Mean Effective Velocity and TI Distributions - (a) VR=0.5 and (b) VR=1.0

25

Adiabatic Effectiveness: SHUP Injection

Figure 6 highlights the general shape and magnitudes of effectiveness distributions for short-hole injection at the two VR's. Intersections of grid lines in the figure correspond to measurement locations. Several lateral distributions of η for the two cases are provided in Fig. 8. The largest values of adiabatic effectiveness are near the downstream edge of the hole and along the hole centerline. Values decay continuously in both the streamwise and lateral directions, indicating no jet detachment (to be discussed). The lower velocity ratio case yields higher effectiveness in this 12% FSTI situation. The major difference with VR is a broader distribution in the lateral direction for VR=0.5 than with VR=1.0. Figure 7 shows that results are consistent with other high-FSTI data in the literature when hole L/D and coolant-to-freestream momentum flux ratios are matched. Several researchers, including Sinha et al. (1991), have documented that the momentum flux ratio, I, can be useful for scaling effectiveness results - noting that for low blowing rates, adiabatic effectiveness scales on the blowing mass flux ratio (and momentum flux ratios with only slightly worse agreement) whereas, at high blowing rates (I>0.5), scaling on I is most effective (with a mild effect of density ratio).

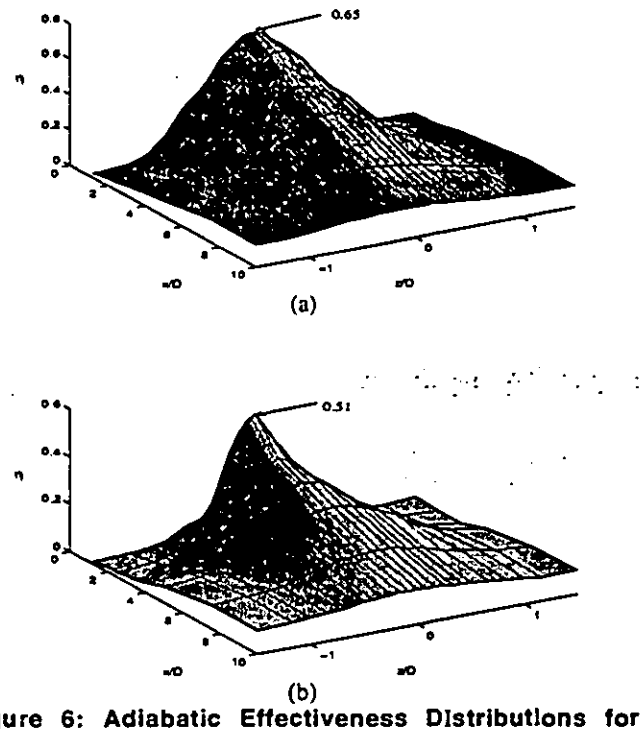

Figure 6: Adiabatic Effectiveness Distributions for Short-Hole Injection at (a) VR=0.5 and (b) VR=1.0

Adiabatic Effectiveness: LHUP Injection.

Centerline adiabatic effectiveness comparisons are made in Fig. 7 for long-hole injection versus short-hole injection. At VR=0.5, the two are similar. Short-hole injection exhibits slightly higher η in the very near-hole region (x/D<2.5). At VR=1.0, a definite detachment of the coolant jet in the near-hole region is visible with long-hole injection; the centerline value rises from x/D=1.25 to x/D=2.5. Downstream, the long-hole case has higher effectiveness values relative to the short-hole case. The reduced jetting of the long-hole case has apparently allowed more of the coolant to be turned streamwise, resulting in reduced mixing of the freestream and higher effectiveness values downstream of reattachment. The effectiveness data presented for short and long holes complement the data presented by Burd et al. (1996).

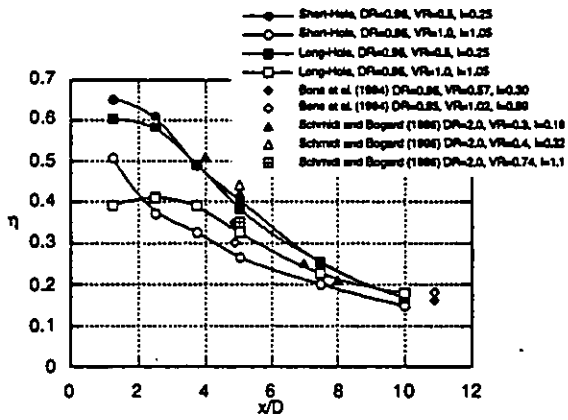

Figure 7: Centerline Adiabatic Effectiveness for Short-Hole and Long-Hole Injection
Bons et al. (1994)-L/D=3.5, FSTI=11.5%, 35°-Inclination
Schmidt and Bogard (1996)-L/D=6.0, FSTI=10%, 30°-Inclination

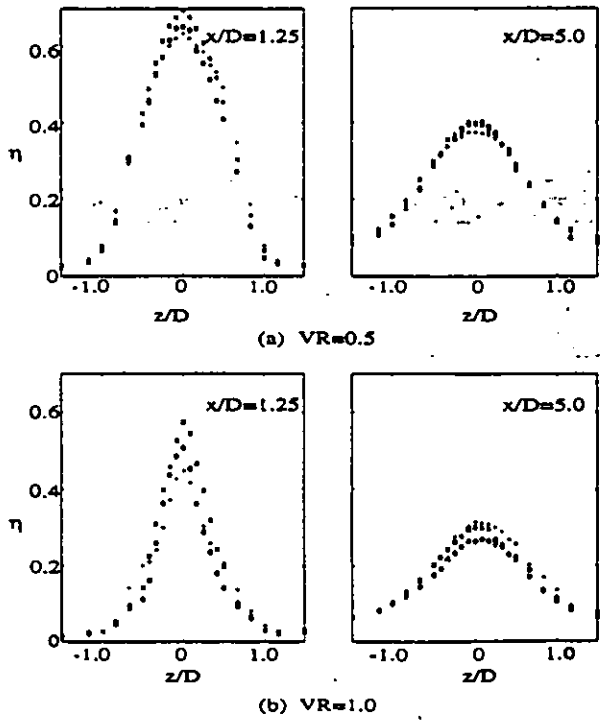

Figure 8: Local Adiabatic Effectiveness Distributions with Short Holes at x/D=1.25 and x/D=5.0 with (a) VR=0.5 and (b) VR=1.0
[*=Counter-Flow, o=SHUP, +=Co-Flow]

25

Hole-Exit Profiles: Counter-Flow Delivery

With counter-flow delivery at VR=0.5, mean effective velocity distributions are similar to those of the SHUP case (Fig. 9a). For most of the centerline profiles, differences between counter-flow delivery and the SHUP injection are not significant, with counter-flow exhibiting only slightly higher magnitudes in the region from $-0.5<x/D<0.5$. With VR=1.0, though, the differences are quite substantial. Counter-flow delivery greatly enhances jetting (higher velocities for $x/D<0.5$, Fig. 9b). For $x/D\geq0.5$, however, velocities are very similar to SHUP values.

Effective centerline TI distributions at the two VR's (Fig. 9) show, generally, higher TI levels at locations of lower velocity. TI magnitudes are slightly higher than those for SHUP injection for both VR's over the entire centerline profile.

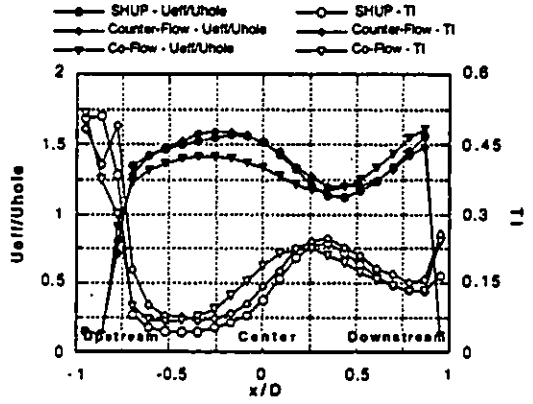

(a)

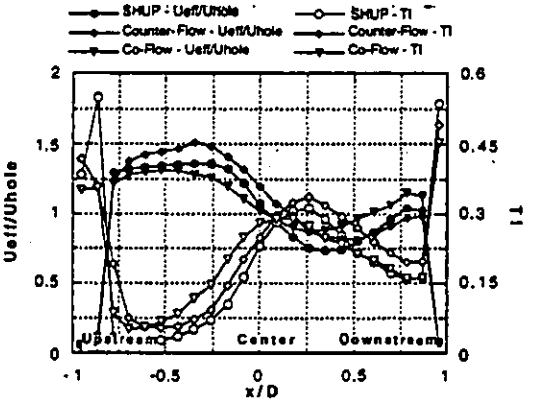

(b)

Figure 9: Comparisons of Normalized Centerline Mean Effective Velocity and TI Distributions - (a) VR=0.5 and (b) VR=1.0 - Short Holes with Unrestricted and with Restricted Plenum Delivery

Hole-Exit Profiles: Co-Flow Delivery

The general shape of the effective velocity distribution found with the SHUP is still apparent with co-flow delivery. With VR=0.5 (Fig. 9a), magnitudes of the normalized mean effective velocities are noticeably lower in the upstream portion of the jet exit plane with co-flow delivery than with SHUP, however. The velocities at the downstream edge of the holes ($x/D>0.5$) are slightly higher. Also, the depression in the velocity profile has shifted upstream to $x/D=0.3$ versus $x/D=0.4$ for the SHUP counterpart. With VR=1.0 (Fig. 9b), nearly the same effective velocity behavior is observed - lower velocities in the upstream portion and higher velocities in the downstream portion of the hole exit. For this case, though, the differences in the downstream portion of the profile are more prominent.

TI distributions (Figs. 9a and 9b) show comparable magnitudes to those with the SHUP but slightly higher values at the upstream portion of the film cooling exit plane. As with no plenum restriction and counter-flow delivery, TI levels are inversely related to the effective velocities.

Adiabatic Effectiveness: Counter-Flow Delivery

With VR=0.5 and along the hole centerline (Fig. 10), counter-flow delivery is the most effective configuration in the near-hole region ($x/D=1.25$) but it quickly loses this advantage downstream. From $2.5\leq x/D\leq10.0$, counter-flow delivery is very similar to unrestricted plenum injection and co-flow delivery. Although centerline values are higher in the near-hole region, the laterally-averaged effectiveness values (Fig. 11) are comparable to short-hole injection at all streamwise positions.

For VR=1.0 and along the centerline (Fig. 10), counter-flow delivery exhibits the highest magnitude of effectiveness in the near-hole region. At $x/D=1.25$, for instance, η for counter-flow delivery is 57% whereas it is only about 51% for the SHUP case. In moving downstream, counter-flow delivery continues to be more effective than without restriction. This higher effectiveness is again observed in the laterally-averaged data (Fig. 11), but to a lesser degree.

Adiabatic Effectiveness: Co-Flow Delivery

Co-flow injection shows little substantive differences in centerline (Fig. 10) and laterally-averaged (Fig. 11) effectiveness in comparison to the SHUP case at VR=0.5. At most, it appears to have slightly lower centerline effectiveness values in the near-hole region. At VR=1.0, the situation is different. In the near-wall region ($x/D=1.25$), centerline η values (Fig. 10) are substantially lower for co-flow delivery than they are for counter-flow delivery and SHUP flow. Instead of there being a rapid decay when moving in the streamwise direction, it decays more slowly ($x/D<3.75$). Co-flow delivery also undergoes a substantial streamwise change relative to the other delivery configurations. In the near-hole region, co-flow is least effective ($x/D=1.25$), increasing in relative effectiveness until it is the most effective scheme ($x/D=3.75$). From $x/D=3.75$ to 10, co-flow remains more effective than delivery without restriction but at a level nearly the same as with counter-flow delivery. This behavior indicates a potential detachment of the film cooling jet in the near-hole region at high VR. No detachment was apparent with counter-flow and in the SHUP case. Co-flow delivery has a more uniform hole-exit profile with higher velocities in the downstream portion of the hole (Fig. 9b) than for the other cases. At a high VR, these higher velocities lead to

separation, then reattachment, of the coolant. While detached, the centerline effectiveness is lower than had it not detached. Downstream from the point of reattachment, higher centerline η values are observed, as with long-hole injection. In terms of laterally-averaged effectiveness (Fig. 11), co-flow delivery is consistently more effective than, or equal to, the SHUP case, even in the region of jet detachment.

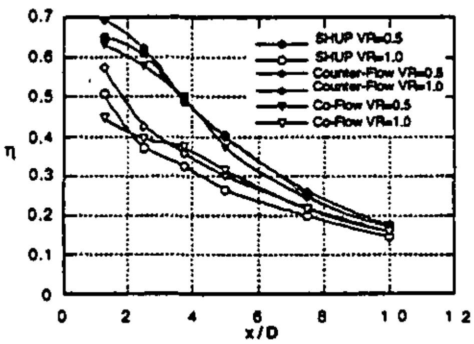

Figure 10: Centerline Adiabatic Effectiveness Distributions (a) VR=0.5 and (b) VR=1.0

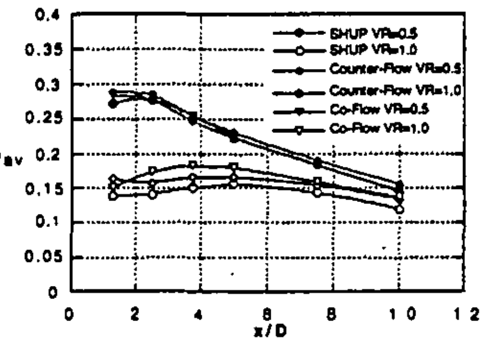

Figure 11: Laterally-Averaged Adiabatic Effectiveness Distributions (a) VR=0.5 and (b) VR=1.0

FLOW PATTERN SPECULATIONS

The present results document the influences of the plenum geometry and hole length on film cooling. Long-hole injection is visibly different than short-hole injection. The two result in distinctly dissimilar exit profiles and effectiveness distributions. In comparison to SHUP injection, coolant flow with counter-flow delivery exits with more momentum at the upstream portion of the film cooling hole causing a blockage of the freestream flow. This coolant flow is rapidly redirected into the streamwise direction by the interaction with the freestream, however. This redirection and interaction with the freestream leads to higher effective velocities in the downstream portion of the hole exit and higher centerline effectiveness values in the near-hole region. Co-flow delivery tends to have a more uniform hole-exit profile and more momentum in the downstream portion of the hole exit, compared to SHUP injection. The net result of co-flow delivery, however, varies with the velocity ratio. At high VR, the higher momentum of the flow in the downstream portion of the hole leads to detachment of the jet and lower centerline effectiveness values in the near-hole region, but higher centerline effectiveness values farther downstream. Figure 12 depicts the speculated flow streamlines along the hole centerlines.

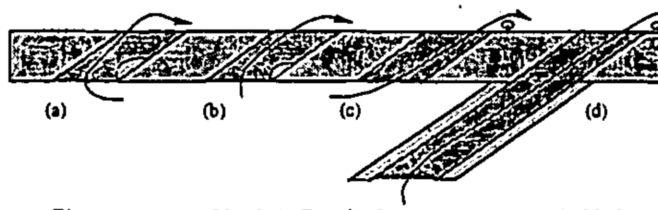

Figure 12 : Model Depicting Speculated Major Centerline Flow Streamlines for Different Geometries Studied - (a) Counter-Flow; (b) Short-Hole, Unrestricted - SHUP;(c) Co-Flow; and (d) Long-Hole, Unrestricted-LHUP

A common feature of the cases with L/D=2.3 is the jetting observed in the hole-exit profiles. Two plausible mechanisms, inertia and ingested vorticity, may be responsible for this jetting. In terms of inertial influences, it may be argued that jetting results from a vena contracta that develops in the hole entrance (Burd et al., 1996; Leylek and Zerkle, 1994). For all configurations in this study, the inertia of the film cooling supply flow coupled with the hole inclination angle, would likely create zones of separation near the entrances to the holes, similar to those shown in Fig. 12. These separation zones would, thus, create a vena contracta in this region. Alternatively, in studying internal plenum heat transfer, Byerley et al. (1988, 1992) discussed the effect of vorticity within the boundary layer of the film cooling flow approaching the holes (bottom surface of Fig. 12). A study of this vorticity and its ingestion into the film cooling hole would show that it tends to create a secondary flow pattern in the hole that leads to higher velocities on the upstream side of the hole (relative to the freestream) for cases (a) and (b) in Fig. 12 and higher velocities in the downstream side of the hole for case (c). This is the trend shown in the measurements (Fig. 9). The relative influences of inertia and vorticity ingested into the hole on the exit profile distribution is not known.

CONCLUDING REMARKS

A very useful technique for measuring adiabatic effectiveness of film cooling with a traversing thermocouple in the flow has been implemented. The technique is attractive in its simplicity and in that it provides temperature profile information over the point where the effectiveness is measured.

Measurements document that both hole-exit profiles and surface adiabatic effectiveness values are influenced by the cooling hole length and delivery plenum geometry. The flow delivery configuration, hole L/D, and velocity ratio effects are documented. The effects cannot be correlated in a simplistic way. It is noted, however, that long- versus short-hole injection is a more important

25

distinction than the various means of delivery of the flow to the holes. The plenum geometry does have an effect on the film cooling performance, with the differences between cases amplified at the higher velocity ratio.

Comparisons of centerline and laterally-averaged effectiveness values suggest that the overall manner in which the coolant interacts with the freestream and then protects the surface is fundamentally different with each of the cases.

Flow patterns for the various flow situations have been suggested. They emphasize the fundamental differences between the cases investigated and are consistent with the data.

ACKNOWLEDGMENTS

This work is part of the NASA-Lewis Research Center Advanced Subsonic Technology Program. The Project Monitor is Douglas Thurman.

REFERENCES

Berhe, M. K. and Patankar, S. V., 1996, "A Numerical Study of Discrete-Hole Film Cooling," ASME Paper 96-WA/HT-8.

Blackwell, B. F. and Moffat, R. J., 1975, "Design and Construction of a Low-Velocity Boundary Layer Temperature Probe," J. Heat Transfer, May, pp. 313-315.

Bons, J. P., MacArthur, C. D., and Rivir, R. B., 1994, "The Effect of High Freestream Turbulence of Film Cooling Effectiveness," ASME Paper 94-GT-51.

Brown, A. and Minty, A. G., 1975, "The Effects of Mainstream Turbulence Intensity and Pressure Gradient on Film Cooling Effectiveness for Cold Air Injection Slits of Various Ratios," ASME Paper 75-WA/HT-17.

Brown, A. and Saluja, C. A., 1979, "Film Cooling from Three Rows of Holes on an Adiabatic Constant Heat Flux and Isothermal Surfaces in the Presence of Variable Free-Stream Velocity Gradients and Turbulence Intensity," ASME Paper 79-GT-24.

Burd, S. W., Kaszeta, R. W., and Simon, T. W., 1996, "Measurements in Film Cooling Flows: Hole L/D and Turbulence Intensity Effects," ASME Paper 96-WA/HT-7.

Byerley, A. R., Jones, T. V., and Ireland, P. T., 1988, "Detailed Heat Transfer Measurements Near and Within the Entrance of a Film Cooling Hole," ASME Paper 88-GT-155.

Byerley, A. R., Jones, T. V., and Ireland, P. T., 1992, "Internal Passage Heat Transfer Near the Entrance to a Film Cooling Hole: Experimental and Computational Results," ASME Paper 92-GT-241.

Gillespie, D. R. H., Byerley, A. R., Ireland, P. T., Wang, Z., and Jones, T. V., 1994, "Detailed Measurements of Local Heat Transfer Coefficient at the Entrance to Normal and Inclined Film Cooling Holes," ASME Paper 94-GT-1.

Goebel, S. G., Abuaf, N., Lovett, J. A., and Lee, C.-P., 1993, "Measurements of Combustor Velocity and Turbulence Profiles," ASME Paper 93-GT-228.

Gogineni, S. P., Rivir, R. B., Pestian, D. J., and Goss, L. P., 1996, "PIV Measurements of Flat Plate Film Cooling Flow with High Free Stream Turbulence," AIAA Paper 96-0617.

Jumper, G. W., Elrod, W. C., and Rivir, R. B., 1991, "Film Cooling Effectiveness in High-Turbulence Flow," J. Turbomachinery, Vol. 113, pp. 479-483.

Kline, S. J. and McClintock, F. A., 1953, "Describing Uncertainties in Single-Sample Experiments, Mech. Eng., January, pp. 3-8.

Kohli, A. and Bogard, D. G., 1995, "Adiabatic Effectiveness, Thermal Fields, and Velocity Fields for Film Cooling with Large Angle Injection," ASME Paper 95-GT-219.

Laufer, J., 1953," The Structure of Turbulence in Fully-Developed Pipe Flow," NACA Report 1174.

Launder, B. E. and York, J., 1974, "Discrete-Hole Cooling in the Presence of Free Stream Turbulence and Strong Favorable Pressure Gradients," Int. J. Heat Mass Transfer, Vol. 17, pp. 1403-1409.

Leylek J. H. and Zerkle R. D., 1994, "Discrete-Jet Film Cooling: A Comparison of Computational Results with Experiments," J. Turbomachinery, Vol. 116, pp. 358-368.

MacMullin, R., Elrod, W. C., and Rivir, R. B., 1989, "Free Stream Turbulence from a Circular Wall Jet on Flat Plate Heat Transfer and Boundary Layer Flow," J. Turbomachinery, Vol. 111, pp. 78-86.

Mehendale, A. B. and Han, J. C., 1990, "Influence of High Mainstream Turbulence on Leading Edge Film Cooling Heat Transfer," ASME Paper 90-GT-9.

Pietrzyk, J. R., Bogard, D. G., and Crawford, M. E., 1989, "Hydrodynamic Measurements of Jets in a Crossflow for Gas Turbine Film Cooling Applications," J. Turbomachinery, Vol. 111, pp. 139-145.

Pietrzyk, J. R., Bogard, D. G., and Crawford, M. E., 1990, "Effects of Density Ratio on the Hydrodynamics of Film Cooling," J. Turbomachinery, Vol. 112, pp. 437-443.

Schmidt, D. L. and Bogard, D. G., 1996, "Effects of Free-Stream Turbulence and Surface Roughness on Film Cooling," ASME Paper 96-GT-462.

Schmidt, D. L., Sen, B., and Bogard, D. G., 1994, "Film Cooling with Compound Angle Holes: Adiabatic Effectiveness," ASME Paper 94-GT-312.

Sinha, A. K., Bogard, D. G., and Crawford, M. E., 1991, "Film Cooling Effectiveness of a Single Row of Holes with Variable Density Ratio," J. Turbomachinery, Vol. 113, pp. 442-449.

Thole, K. A., Gritsch, M., Schulz, A., and Wittig, S., 1996a, "Effect of a Crossflow at the Entrance to a Film Cooling Hole," Accepted to J. Fluids Engineering.

Thole, K. A., Gritsch, M., Schulz, A., and Wittig, S., 1996b, "Flowfield Measurements for Film Cooling Holes with Expanded Exits," ASME Paper 96-GT-174.

Wang, L., Tsang, H., Simon, T. W., and Eckert, E. R. G., 1996, "Measurements of Mean Flow and Eddy Transport over a Film Cooled Surface," ASME-HTD, Vol. 327, pp. 71-79.

Wittig, S., Schulz, A., Gritsch, M., and Thole, K. A., 1996, "Transonic Film Cooling Investigations: Effects of Hole Shapes and Orientations," ASME Paper 96-GT-222.

Yavuzkurt, S., 1984, "A Guide to Uncertainty Analysis of Hot-Wire Data," J. Fluids Engineering, June, Vol. 106, pp. 181-186.

You, S. M., 1986, "Turbulent Boundary Layer Heat Transfer and Fluid Mechanics Measurements on a Curved Convex Wall," M.S. Thesis, Dept. Mech. Eng., University of Minnesota.